

# Coupling and Dissociation in Artificial Molecules

Constantine Yannouleas<sup>a</sup> and Uzi Landman

School of Physics, Georgia Institute of Technology, Atlanta, GA 30332-0430

Received: December 19, 2000 / Revised version: date

**Abstract.** We show that the spin-and-space unrestricted Hartree-Fock method, in conjunction with the companion step of the restoration of spin and space symmetries via Projection Techniques (when such symmetries are broken), is able to describe the full range of couplings in two-dimensional double quantum dots, from the strong-coupling regime exhibiting delocalized molecular orbitals to the weak-coupling and dissociation regimes associated with a Generalized Valence Bond combination of atomic-type orbitals localized on the individual dots. The weak-coupling regime is always accompanied by an antiferromagnetic ordering of the spins of the individual dots. The cases of dihydrogen ( $H_2$ , 2e) and dilithium ( $Li_2$ , 6e) quantum dot molecules are discussed in detail.

PACS. 73.21.La Quantum dots { 85.35.-p Nanoelectronic devices { 31.15.Rh Valence bond calculations

## 1 Introduction

Two-dimensional (2D) Quantum Dots (QD's) are usually referred to as artificial atoms, a term suggestive of strong similarities between these manmade devices and the physical behavior of natural atoms. As a result, in the last few years, an intensive theoretical effort [1,2,3,4,5,6,7,8,9,10] has been devoted towards the elucidation of the appropriate analogies and/or differences. Recently, we have shown [7,8,9] that, even in the absence of a magnetic field, the most promising analogies are found mainly outside the confines of the central-field approximation underlying the Independent-Particle Model (IPM) and the ensuing physical picture of electronic shells and the Aufbau Principle. Indeed, as a result of the lower electronic densities in QD's, strong electron correlations can lead (as a function of the ratio  $R_w$  between the interelectron repulsion and the zero-point kinetic energy) to a drastically different physical regime, where the electrons become localized, arranging themselves in concentric geometric shells and forming electron molecules. In this context, it was found [8,9] that the proper analogy for the particular case of a 2e QD is the collective-motion picture reminiscent of the vibrating and rather exotic phenomena of the doubly-excited natural helium atom, where the emergence of a "loppy" trimeric molecule (consisting of the two localized electrons and the heavy  $\alpha$ -particle nucleus) has been well established [11,12].

A natural extension of this theoretical effort has also developed in the direction of lateral 2D QD Molecules (QDM's, often referred to as artificial molecules), aiming at elucidating [7,10,13,14,15,16] the analogies and differences

between such artificially fabricated nanostructures and the natural molecules.

In this paper, we address the interplay of coupling and dissociation in QDM's, and its effects concerning the appearance of ferromagnetic versus antiferromagnetic ordering. We will show that this interplay relates directly to the nature of the coupling in the artificial molecules, and in particular to the question whether such coupling can be described by the Molecular Orbital (MO) Theory or the Valence Bond (VB) Theory in analogy with the chemical bond in natural molecules.

Furthermore, we show that the onset at a moderate interdot barrier or interdot distance  $d_0$ , as well as the permanency for all separations  $d > d_0$ , of spontaneous magnetization and ferromagnetic ordering predicted for Double QD's by local-spin-density (LSD) calculations [13,14] is an artifact of the MO structure implicit in the framework of these density-functional calculations.

We utilize a self-consistent-field theory which can go beyond the MO approximation, namely the spin-and-space unrestricted Hartree-Fock (SS-UHF), which was introduced by us [7,8] for the description of the many-body problem of both single [7,8] and molecular [7] QD's. This SS-UHF employs  $N$  (where  $N$  is the number of electrons) orbital-dependent, effective (mean-field) potentials and it differs from the more familiar [17] restricted HF (RHF) in two ways: (i) it relaxes the double-occupancy requirement, namely, it employs different spatial orbitals for the two different (i.e., the up and down) spin directions  $\uparrow$  and  $\downarrow$ , thus the designation "spin (S) unrestricted", and (ii) it relaxes the requirement that the electron orbitals be constrained by the symmetry of the external confining field [thus the designation "space (S) unrestricted"].

<sup>a</sup> e-mail: constantine.yannouleas@physics.gatech.edu

In this paper we will show that the solutions with broken space symmetry allowed in QDM's by the sS-UHF provide a natural vehicle for formulating a Generalized Valence Bond (GVB) theory. Furthermore, they result in an antiferromagnetic ordering of the molecular ground state, in contrast to the ferromagnetic ordering of the MO method which is associated with HF solutions that preserve the space symmetry, namely those derived from the fully restricted Hartree-Fock (RHF) or the spin-unrestricted (but not space-unrestricted) Hartree-Fock (s-UHF) approaches.

## 2 The two-center-oscillator confining potential

In the 2D two-center-oscillator (TCO), the single-particle levels associated with the confining potential of the artificial molecule are determined by the single-particle hamiltonian [18]

$$H = T + \frac{1}{2}m^{-1}_x x^2 + \frac{1}{2}m^{-1}_{yk} Y_k^2 + V_{\text{neck}}(y) + h_k + \frac{g}{h} \frac{B}{B_0} S; \quad (1)$$

where  $y_k^0 = y - y_k$  with  $k = 1$  for  $y < 0$  (left) and  $k = 2$  for  $y > 0$  (right), and the  $h_k$ 's control the relative well-depth, thus allowing studies of hetero-QDM's.  $x$  denotes the coordinate perpendicular to the interdot axis ( $y$ ).  $T = (\hbar^2/2m)(\partial/\partial x)^2$ , with  $A = 0.5(B_y/B_x; 0)$ , and the last term in Eq. (1) is the Zeeman interaction with  $g$  being the effective  $g$  factor and  $B_0$  the Bohr magneton. Here we limit ourselves to systems with  $\hbar\omega_{x1} = \hbar\omega_{x2} = \hbar\omega_x$ . The most general shapes described by  $H$  are two semiellipses connected by a smooth neck  $V_{\text{neck}}(y)$ .  $y_1 < 0$  and  $y_2 > 0$  are the centers of these semiellipses,  $d = y_2 - y_1$  is the interdot distance, and  $m$  is the effective electron mass.

For the smooth neck, we use  $V_{\text{neck}}(y) = \frac{1}{2}m^{-1}_{yk} [c_k y_k^3 + d_k y_k^4]$  ( $y_j = y - y_k$ ), where  $(u) = 0$  for  $u > 0$  and  $(u) = 1$  for  $u < 0$ . The four constants  $c_k$  and  $d_k$  can be expressed via two parameters, as follows:  $(1)^k c_k = (2/4)^{b_k} y_k$  and  $d_k = (1/3)^{b_k} y_k^2$ , where the barrier-control parameters  $b_k = (V_b - h_k)/V_{0k}$  are related to the actual (controllable) height of the bare barrier ( $V_b$ ) between the two QD's, and  $V_{0k} = m^{-1}_{yk} y_k^2/2$  (for  $h_1 = h_2$ ,  $V_{01} = V_{02} = V_0$ ).

The single-particle levels of  $H$ ; including an external perpendicular magnetic field  $B$ , are obtained by numerical diagonalization in a (variable-with-separation) basis consisting of the eigenstates of the auxiliary hamiltonian:

$$H_0 = \frac{p^2}{2m} + \frac{1}{2}m^{-1}_x x^2 + \frac{1}{2}m^{-1}_{yk} Y_k^2 + h_k; \quad (2)$$

This eigenvalue problem is separable in  $x$  and  $y$ , i.e., the wave functions are written as  $\psi_m(x; y) = X_m(x)Y(y)$ . The solutions for  $X_m(x)$  are those of a one-dimensional oscillator, and for  $Y(y)$  they can be expressed through the parabolic cylinder functions [18]  $U[\frac{1}{2}k; (1)^k y_k]$ , where  $k = y_k^0/2m^{-1}_{yk} \hbar\omega_x$ ,  $k = (E_y + h_k)/(\hbar\omega_x)$ , and  $E_y =$

$(+0.5)\hbar\omega_{y1} + h_1$  denotes the  $y$ -eigenvalues. The matching conditions at  $y = 0$  for the left and right domains yield the  $y$ -eigenvalues and the eigenfunctions  $Y(y)$  ( $m$  is integer and  $\psi$  is in general real).

In this paper, we will focus on the zero-field case ( $B = 0$ ) and we will limit ourselves to symmetric (homopolar) QDM's, i.e.,  $\hbar\omega_x = \hbar\omega_{y1} = \hbar\omega_{y2} = \hbar\omega_y$ , with equal well-depths of the left and right dots, i.e.,  $h_1 = h_2 = 0$ . In all cases, we will use  $\hbar\omega_y = 5$  meV and  $m = 0.067m_e$  (this effective-mass value corresponds to GaAs).

## 3 The Many-Body Hamiltonian

The many-body hamiltonian  $H$  for a dimeric QDM comprising  $N$  electrons can be expressed as a sum of the single-particle part  $H(i)$  defined in Eq. (1) and the two-particle interelectron Coulomb repulsion,

$$H = \sum_{i=1}^N H(i) + \sum_{i=1}^N \sum_{j>i}^N \frac{e^2}{\epsilon r_{ij}}; \quad (3)$$

where  $\epsilon$  is the dielectric constant and  $r_{ij}$  denotes the relative distance between the  $i$  and  $j$  electrons.

As we mentioned in the introduction, we will use the sS-UHF method for determining at a first level an approximate solution of the many-body problem specified by the hamiltonian (3). The sS-UHF equations were solved in the Pople-Nesbet-Roothaan formalism [19] using the interdot-distance adjustable basis formed with the eigenfunctions  $\psi_m(x; y)$  of the TCO defined in section 2.

As we will explicitly illustrate in section 5 for the case of the  $H_2$ -QDM, the next step in improving the sS-UHF solution involves the use of Projection Techniques in relation to the UHF single Slater determinant.

## 4 A first example of a homopolar two-dimensional artificial molecule: the lateral $Li_2$ -QDM

As an illustrative example, we consider here an open-shell ( $N = 6$  electrons) QDM made of two QD's (hence the name  $Li_2$ -QDM), with an interdot distance of  $d = 70$  nm and an interdot barrier height of  $V_b = 10$  meV. The value of the dielectric constant is first taken to be  $\epsilon = 20.0$ . This value is higher than the value ( $\epsilon(\text{GaAs}) = 12.9$  for GaAs) and may be viewed as resulting from screening produced by the external charges residing in the gates and/or the finite height (in the  $z$  direction) of the dot. This value of  $\epsilon$  is chosen such that the electron repulsion is not strong enough to precipitate individual electron localization [20] within each individual dot (that is, to inhibit Wigner crystallization on each of the dots, see Ref. [7]). This example thus conforms better to the case of a natural  $Li_2$  molecule. It was earlier presented briefly in Ref. [7] in connection with the formation of electron puddles (EP's). Here we will

## FIGURE 1

Fig. 1. Lateral  $\text{Li}_2$ -QDM : s-UHF spin-up occupied orbitals (modulus square) and total charge (CD) and spin (SD) densities (top row) for the  $P = 2$  spin polarized case. The numbers displayed with each orbital are their s-UHF eigenenergies in meV. The two spin-down orbitals are not displayed; they are similar to the  $\phi_g$  and the  $\phi_u$  and have energies of 17.10 meV and 17.27 meV, respectively. The number displayed with the total charge density (top left) is the s-UHF total energy in meV. Distances are in nm and the electron densities in  $10^4 \text{ nm}^{-2}$ . The choice of parameters is:  $m^* = 0.067m_e$ ,  $\hbar\omega_0 = 5 \text{ meV}$ ,  $d = 70 \text{ nm}$ ,  $V_b = 10 \text{ meV}$ ,  $\epsilon = 20$ .

## FIGURE 2

Fig. 2. Lateral  $\text{Li}_2$ -QDM : RHF occupied orbitals (modulus square) and charge (CD) and spin (SD) densities (top row) for the  $P = 0$  spin unpolarized case. The numbers displayed with each orbital are their RHF eigenenergies in meV, while the up and down arrows indicate electrons with up or down spin, respectively. The number displayed with the total charge density is the RHF total energy in meV. Distances are in nm and the electron densities in  $10^4 \text{ nm}^{-2}$ . The choice of parameters is the same as in Fig. 1.

present a detailed study of it by contrasting the descriptions resulting from both the space-symmetry preserving (RHF or s-UHF) and non-preserving (ss-UHF) methods.

We start by presenting HF results which preserve the space symmetry of the QDM; the results corresponding to

the  $P = N - N_{\text{#}} = 2$  and the  $P = 0$  spin polarizations are displayed in Fig. 1 and Fig. 2, respectively. The  $P = 2$  case is an open-shell case and is treated within the (spin unrestricted) s-UHF method, in analogy with the standard practice for open-shell configurations in Quantum Chemistry [21]; the  $P = 0$  case is of a closed-shell-type and is treated within the RHF approach.

The corresponding energies are  $E_{\text{sUHF}}(P = 2) = 74.137 \text{ meV}$  and  $E_{\text{RHF}}(P = 0) = 75.515 \text{ meV}$ , i.e., the space-symmetry preserving HF variants predict that the polarized state is the ground state of the molecule. Indeed, by preserving the symmetries of the confining potential, the associated orbitals are clearly of the MO-type. In this MO picture the  $\text{Li}_2$ -QDM exhibits an open shell structure (for 2D QDM's, the closed shells correspond to  $N = 4; 12; 24; \dots$  electrons, that is shell closures at twice the values corresponding to an individual harmonic 2D QD) and thus Hund's first rule should apply for the two electrons outside the core closed shell of the first 4 electrons.

Fig. 1 displays for the  $P = 2$  spin polarization the four occupied spin-up s-UHF orbitals ( $\phi_g, \phi_u, \phi_{xg}, \phi_{xu}$ ), as well as (top of Fig. 1) the total charge density (CD, sum of the  $N - N_{\text{#}}$  electron densities) and spin density (SD, difference of the  $N - N_{\text{#}}$  electron densities). The two occupied spin-down orbitals ( $\phi_g, \phi_u$ ) are not shown: in conforming with the DODS approximation, they are slightly different from the  $\phi_g$  and  $\phi_u$  ones.

Fig. 2 displays the corresponding quantities for the  $P = 0$  case. In both (the  $P = 2$  and  $P = 0$ ) cases, the orbitals are clearly molecular orbitals delocalized over the whole QDM. The  $P = 2$  polarization (Fig. 1) exhibits the molecular configuration  $\begin{smallmatrix} 1 & 0 & 1 & 0 & 1 & 1 \\ \phi_g & \phi_g & \phi_u & \phi_u & \phi_{xg} & \phi_{xu} \end{smallmatrix}$ ; this configuration changes to  $\begin{smallmatrix} 2 & 2 & 2 \\ \phi_g & \phi_u & \phi_{yg} \end{smallmatrix}$  in the  $P = 0$  case (Fig. 2).

Fig. 3 displays the corresponding quantities for the  $P = 0$  state calculated using the (spin-and-space unrestricted) ss-UHF. This state exhibits a breaking of space symmetry (the reflection symmetry between the left and right dot). Unlike the MO's of the  $P = 0$  RHF solution (Fig. 2), the ss-UHF orbitals in Fig. 3 are well localized on either one of the two individual QD's and strongly resemble the atomic orbitals (AO's) of an individual  $\text{Li}$ -QD, i.e., they are of  $1s$  and  $1p_x$  type. Comparing with the MO case of Fig. 2, one sees that the symmetry breaking did not greatly influence the total charge density. However, a dramatic change appeared regarding the spin densities. Indeed the SD of the ss-UHF solution (see top right of Fig. 3) exhibits a prominent spin density wave (SDW) associated with an antiferromagnetic ordering of the coupled individual QD's. Formation of such SDW ground states in QDM's is accompanied by electron (orbital) localization on the individual dots, and thus in Ref. [7] we proposed for them the name of Electron Puddles (EP's). Notice that the EP's represent a separate class of symmetry broken solutions, different [7] from the SDW's that can develop within a single QD [22] and whose formation involves the relative rotation of delocalized open-shell orbitals, instead of electron localization.

The ss-UHF total energy for the  $P = 0$  unpolarized case is  $E_{\text{ssUHF}}(P = 0) = 74.136 \text{ meV}$ , i.e., the sym-

FIGURE 3

FIGURE 4

Fig. 3. Lateral  $\text{Li}_2$ -QDM: sS-UHF occupied orbitals (modulus square) and charge (CD) and spin (SD) densities (top row) for the  $P = 0$  spin unpolarized case. The numbers displayed with each orbital are their sS-UHF eigenenergies in meV, while the up and down arrows indicate an electron with an up or down spin. The number displayed with the charge density is the sS-UHF total energy in meV. Distances are in nm and the electron densities in  $10^4 \text{ nm}^{-2}$ . The choice of parameters is the same as in Fig. 1.

metry breaking produces a remarkable gain in energy of 1.379 meV. As a result, the unpolarized state is the ground state, while the ferromagnetic ordering predicted by the RHF is revealed to be simply an artifact of the MO structure implicit in this level of approximation. Notice that the symmetry-broken unpolarized state is only 0.001 meV lower in energy than the  $P = 2$  polarized one, namely the two states are practically degenerate, which implies that for the set of parameters employed here the QDM molecule is located well in the dissociation regime.

Although the symmetry breaking within the HF theory allows one to correct for the artifact of the spontaneous polarization exhibited by the MO approaches, i.e., the fact that the MO polarized solutions are the lowest in energy upon separation, the resulting sS-UHF many-body wave function violates both the total spin and the space reflection symmetries. Intuitively further progress can be achieved as follows: the orbitals (see Fig. 3) of the sS-UHF can be viewed as optimized atomic orbitals (OAO's) to be used in constructing a many-body wave function conforming to a Generalized Valence Bond (GVB) structure and exhibiting the correct symmetry properties. Starting with the sS-UHF symmetry-breaking Slater determinant, this program can be systematically carried out within the framework of the theory of Restoration of Symmetry (RS) via the so-called Projection Techniques. Instead of the more complicated case of the  $\text{Li}_2$ -QDM, and for reasons of simplicity and conceptual clarity, we will present below the case of the QDM molecular hydrogen as an illustrative example of this RS procedure.

Fig. 4. Lateral  $\text{H}_2$ -QDM: occupied orbitals (modulus square, bottom half) and total charge (CD) and spin (SD) densities (top half) for the  $P = 0$  spin unpolarized case. Left column: RHF results. Right column: sS-UHF results exhibiting a breaking of the space symmetry. The numbers displayed with each orbital are their eigenenergies in meV, while the up and down arrows indicate an electron with an up or down spin. The numbers displayed with the charge densities are the total energies in meV. Unlike the RHF case, the spin density of the sS-UHF exhibits a well developed spin density wave. Distances are in nm and the electron densities in  $10^4 \text{ nm}^{-2}$ . The choice of parameters is:  $m = 0.067 m_e$ ,  $\hbar\omega_0 = 5 \text{ meV}$ ,  $d = 30 \text{ nm}$ ,  $V_b = 4.95 \text{ meV}$ ,  $\beta = 20$ .

## 5 Artificial molecular hydrogen ( $\text{H}_2$ -QDM) in a Generalized Valence Bond Approach

### 5.1 The sS-UHF description

We turn now to the case of the  $\text{H}_2$ -QDM. Fig. 4 displays the RHF and sS-UHF results for the  $P = 0$  case (singlet) and for an interdot distance  $d = 30 \text{ nm}$  and a barrier  $V_b = 4.95 \text{ meV}$ . In the RHF (Fig. 4, left), both the spin-up and spin-down electrons occupy the same bonding ( $\sigma_g$ ) molecular orbital. In contrast, in the sS-UHF result the spin-up electron occupies an optimized  $1s$  (or  $1s_L$ ) atomic-like orbital (AO) in the left QD, while the spin-down electron occupies the corresponding  $1s^0$  (or  $1s_R$ ) AO in the right QD. Concerning the total energies, the RHF yields  $E_{\text{RHF}}(P = 0) = 13.68 \text{ meV}$ , while the sS-UHF energy is  $E_{\text{sS-UHF}}(P = 0) = 12.83$  representing a gain in energy of 0.85 meV. Since the energy of the triplet is  $E_{\text{sS-UHF}}(P = 1) = E_{\text{sS-UHF}}(P = 1) = 13.01 \text{ meV}$ , the sS-UHF singlet conforms to the requirement that for two electrons at zero magnetic field the singlet is always the ground state; on the other hand the RHF MO solution fails in this respect.

### 5.2 Projected wave function and restoration of the broken symmetry

To make further progress, we utilize the spin projection technique to restore the broken symmetry of the sS-UHF

determinant (henceforth we will drop the prefix  $s$  when referring to the  $s$ S-UHF determinant),

$$\begin{aligned} \frac{1}{2} \bar{P}_{\text{UHF}}(1;2) &= \frac{u(r_1)(1) v(r_1)(1)}{u(r_2)(2) v(r_2)(2)} \\ &= \frac{1}{2} \bar{P}_{\text{UHF}}(1;2) > 0; \end{aligned} \quad (4)$$

where  $u(r)$  and  $v(r)$  are the  $1s$  (left) and  $1s^0$  (right) localized orbitals of the  $s$ S-UHF solution displayed in the right column of Fig. 4; and denote the up and down spins, respectively. In Eq. (4) we also denote a compact notation for the  $\bar{P}_{\text{UHF}}$  determinant, where a bar over a space orbital denotes a spin-down electron; absence of a bar denotes a spin-up electron.

$\bar{P}_{\text{UHF}}(1;2)$  is an eigenstate of the projection  $S_z$  of the total spin  $S = s_1 + s_2$ , but not of  $S^2$ . One can generate a many-body wave function which is an eigenstate of  $S^2$  with eigenvalues  $s(s+1)$  by applying the following projection operator introduced by Lowdin [23,24],

$$P_s = \frac{1}{s(s+1)} \sum_{s^0} \frac{S^2 - s^0(s^0+1)\hbar^2}{[s(s+1) - s^0(s^0+1)\hbar^2]}; \quad (5)$$

where the index  $s^0$  runs over the eigenvalues of  $S^2$ .

The result of  $S^2$  on any UHF determinant can be calculated with the help of the expression,

$$S^2 \bar{P}_{\text{UHF}} = \hbar^2 4(n_{\uparrow} - n_{\downarrow})^2 = 4 + n = 2 + \sum_{i < j} \$_{ij} \bar{P}_{\text{UHF}}; \quad (6)$$

where the operator  $\$_{ij}$  interchanges the spins of electrons  $i$  and  $j$  provided that their spins are different;  $n_{\uparrow}$  and  $n_{\downarrow}$  denote the number of spin-up and spin-down electrons, respectively, while  $n$  denotes the total number of electrons.

For the singlet state of two electrons,  $n_{\uparrow} = n_{\downarrow} = 1$ ,  $n = 2$ , and  $S^2$  has only the two eigenvalues  $s = 0$  and  $s = 1$ . As a result,

$$\begin{aligned} \frac{1}{2} \bar{P}_{2P_0 \text{UHF}}(1;2) &= \frac{1}{2} (\$_{12}) \bar{P}_{\text{UHF}}(1;2) \\ &= \frac{1}{2} \bar{P}_{\text{UHF}}(1;2) > 0; \end{aligned} \quad (7)$$

In contrast to the single-determinantal wave functions of the RHF and  $s$ S-UHF methods, the projected many-body wave function (7) is a linear superposition of two Slater determinants, and thus represents a corrective step beyond the mean-field approximation.

Expanding the determinants in Eq. (7), one finds the equivalent expression

$$2P_0 \text{UHF}(1;2) = (u(r_1)v(r_2) + u(r_2)v(r_1)) (0;0); \quad (8)$$

where the spin eigenfunction for the singlet is given by

$$(s=0; S_z=0) = \frac{1}{\sqrt{2}} (u(1)v(2) - v(1)u(2)) = \frac{1}{\sqrt{2}}; \quad (9)$$

Eq. (8) has the form of a Heitler-London (HL) [25] or valence bond [26,27,28] wave function. However, unlike the HL scheme which uses the orbitals  $\phi_L(r)$  and  $\phi_R(r)$

of the separated (left and right) atoms [29], expression (8) employs the  $s$ S-UHF orbitals which are self-consistently optimized for any separation  $d$  and potential barrier height  $V_b$ . As a result, expression (8) can be characterized as a Generalized Valence Bond (GVB) [30] wave function. Taking into account the normalization of the spatial part, we arrive at the following improved wave function for the singlet state exhibiting all the symmetries of the original many-body hamiltonian,

$$\bar{S}_{\text{GVB}}(1;2) = N_+ \frac{1}{2P_0 \text{UHF}}(1;2); \quad (10)$$

where the normalization constant is given by

$$N_+ = 1 = \frac{1}{1 + S_{uv}^2}; \quad (11)$$

$S_{uv}$  being the overlap integral of the  $u(r)$  and  $v(r)$  orbitals,

$$S_{uv} = \int u(r)v(r)dr; \quad (12)$$

The total energy of the GVB state is given by

$$E_{\text{GVB}}^s = N_+^2 [h_{uu} + h_{vv} + 2S_{uv}h_{uv} + J_{uv} + K_{uv}]; \quad (13)$$

where  $h$  is the single-particle part of the total hamiltonian (1), and  $J$  and  $K$  are the direct and exchange matrix elements associated with the  $e^-e^-$  repulsion  $e^2/r_{12}$ . For comparison, we give also here the corresponding expression for the HF total energy either in the RHF ( $v = u$ ) or  $s$ S-UHF case,

$$E_{\text{HF}}^s = h_{uu} + h_{vv} + J_{uv}; \quad (14)$$

For the triplet, the projected wave function coincides with the original HF determinant, so that the corresponding energies in all three approximation levels are equal, i.e.,  $E_{\text{GVB}}^t = E_{\text{RHF}}^t = E_{\text{UHF}}^t$ .

### 5.3 Comparison of RHF, $s$ S-UHF and GVB results

A major test for the suitability of different methods to the case of QDM's is their ability to properly describe the dissociation limit of the molecule. The  $\text{H}_2$ -QDM dissociates into two non-interacting QD hydrogen atoms with arbitrary spin orientation. As a result, the energy difference,  $\Delta E = E^s - E^t$ , between the singlet and the triplet states of the molecule must approach the zero value from below as the molecule dissociates. To theoretically generate such a dissociation process, we keep the separation  $d$  constant and vary the height of the interdot barrier  $V_b$ ; an increase in the value of  $V_b$  reduces the coupling between the individual dots and for sufficiently high values we can always reach complete dissociation.

Fig. 5 displays the evolution in zero magnetic field of  $\Delta E$  as a function of  $V_b$  and for all three approximation levels, i.e., the RHF (MO Theory, top line), the  $s$ S-UHF (middle line), and the GVB (bottom line). The interdot distance is the same as in Fig. 4, i.e.,  $d = 30$ ; the case of  $d = 20$  is shown at the top panel, while the case of

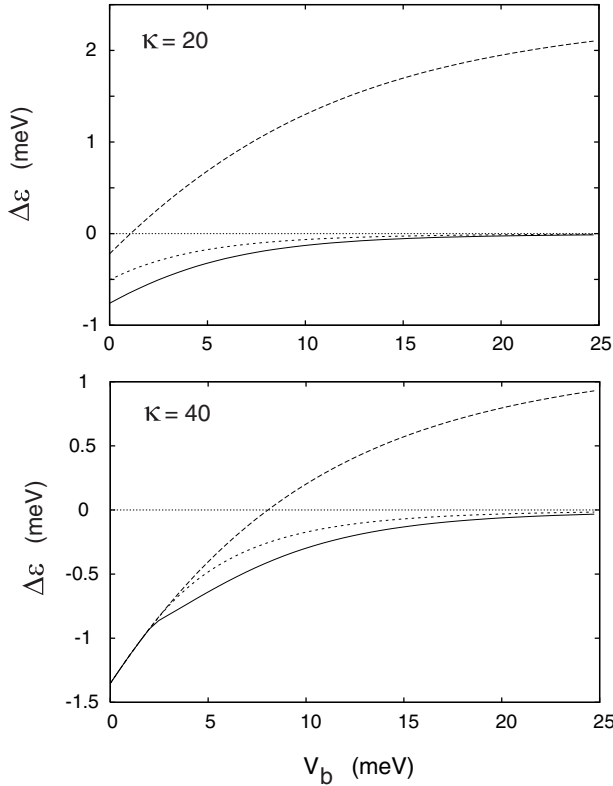


Fig. 5. Lateral  $H_2$ -QDM: The energy difference between the singlet and triplet states according to the RHF (MO Theory, top line), the sS-UHF (middle line), and the GVB approach (Projection Method, bottom line) as a function of the interdot barrier  $V_b$ . For  $V_b = 25$  meV complete dissociation has been clearly reached. Top frame:  $\epsilon = 20$ . Bottom frame:  $\epsilon = 40$ . The choice of the remaining parameters is:  $m = 0.067m_e$ ,  $\hbar\omega_0 = 5$  meV and  $d = 30$  nm.

a weaker e-e repulsion is displayed for  $\epsilon = 40$  at the bottom panel.

We observe first that the MO approach fails completely to describe the dissociation of the  $H_2$ -QDM, since it predicts a strongly stabilized ferromagnetic ordering in contradiction to the expected singlet-triplet degeneracy upon full separation of the individual dots. A second observation is that both the sS-UHF and the GVB solutions describe the dissociation limit ( $\Delta\epsilon \rightarrow 0$  for  $V_b \rightarrow 1$ ) rather well. In particular in both the sS-UHF and the GVB methods the singlet state remains the ground state for all values of the interdot barrier. Between the two singlets, the GVB one is always the lowest, and as a result, the GVB method presents an improvement over the sS-UHF method both at the level of symmetry preservation and the level of energetics.

It is interesting to note that for  $\epsilon = 40$  (weaker e-e repulsion) the sS-UHF and GVB solutions collapse to the MO solution for smaller interdot-barrier values  $V_b \approx 2.8$  meV. However, for the stronger e-e repulsion ( $\epsilon = 20$ ) the sS-UHF and GVB solutions remain energetically well below the MO solution even for  $V_b = 0$ . Since the separa-

ration considered here ( $d = 30$  nm) is a rather moderate one (compared to the value  $d_0 = 28.50$  nm for the extent of the  $1s$  AO), we conclude that there is a large range of materials parameters and interdot distances for which the QDM's are weakly coupled and cannot be described by the MO theory.

## 6 Conclusions

We have shown that the sS-UHF method, in conjunction with the companion step of the restoration of symmetries when such symmetries are broken, is able to describe the full range of couplings in a QDM, from the strong-coupling regime exhibiting delocalized molecular orbitals to the weak-coupling one associated with Heitler-London-type combinations of atomic orbitals.

The breaking of space symmetry within the sS-UHF method is necessary in order to properly describe the weak-coupling and dissociation regimes of QDM's. The breaking of the space symmetry produces optimized atom-like orbitals localized on each individual dot. Further improvement is achieved with the help of Projection Techniques which restore the broken symmetries and yield multi-term in a many-body wave functions. The method of the restoration of symmetry was explicitly illustrated for the case of the molecular hydrogen QDM ( $H_2$ -QDM, see section 5). It led to the introduction of a Generalized Valence Bond many-body wave function as the appropriate vehicle for the description of the weak-coupling and dissociation regimes of artificial molecules. In all instances the weak-coupling regime is accompanied by an antiferromagnetic ordering of the spins of the individual dots.

Additionally, we showed that the RHF, whose orbitals preserve the space symmetries and are delocalized over the whole molecule, is naturally associated with the molecular orbital theory. As a result, and in analogy [26,27,31] with the natural molecules, it was found that the RHF fails to describe the weak-coupling and dissociation regimes of QDM's. It can further be concluded that the spontaneous polarization and ferromagnetic ordering predicted for weakly-coupled double QDM's in Refs. [13,14] is an artifact of the molecular-orbital structure implicit [32] in the framework of LSD calculations.

## References

1. T. Chakraborty, Quantum dots: a survey of the properties of artificial atoms (Elsevier, Amsterdam, 1999).
2. D. P. Farnkuche, V. Gudmundsson, and P. A. Maksym, Phys. Rev. B 47, 2244 (1993).
3. M. Ferconi and G. Vignale, Phys. Rev. B 50, 14722 (1994).
4. K. Hirose and N. S. Wingreen, Phys. Rev. B 59, 4604 (1999).
5. I. H. Lee, V. Rao, R. M. Martin, and J. P. Leburton, Phys. Rev. B 57, 9035 (1998).
6. D. G. Austing, S. Sasaki, S. Tarucha, S. M. Reimann, M. Koskinen, and M. Manninen, Phys. Rev. B 60, 11 514 (1999).

7. C. Yannouleas and U. Landman, *Phys. Rev. Lett.* **82**, 5325 (1999); (E) *ibid.* **85**, 2220 (2000).
8. C. Yannouleas and U. Landman, *Phys. Rev. B* **61**, 15 895 (2000).
9. C. Yannouleas and U. Landman, *Phys. Rev. Lett.* **85**, 1726 (2000).
10. R. N. Barnett, C. L. Cleveland, H. Hakkinen, W. D. Luedtke, C. Yannouleas, and U. Landman, *Eur. Phys. J. D* **9**, 95 (1999).
11. (a) M. E. Kellman and D. R. Herrick, *J. Phys. B* **11**, L755 (1978); (b) *Phys. Rev. A* **22**, 1536 (1980); (c) see also the comprehensive review by M. E. Kellman, *Int. J. Quant. Chem.* **65**, 399 (1997).
12. H.-J. Yuh et al., *Phys. Rev. Lett.* **47**, 497 (1981); G. S. Ezra and R. S. Berry, *Phys. Rev. A* **28**, 1974 (1983); see also review by R. S. Berry, *Contemp. Phys.* **30**, 1 (1989).
13. S. Nagara, J. P. Leburton, and R. M. Martin, *Phys. Rev. B* **60**, 8759 (1999).
14. A. Wensauer, O. Steins, M. Suhrlke, and U. Rossler, *Phys. Rev. B* **62**, 2605 (2000).
15. G. Burkard, D. Loss, and D. P. DiVincenzo, *Phys. Rev. B* **59**, 2070 (1999).
16. X. Hu and S. Das Sarma, *Phys. Rev. A* **61**, 062301 (2000).
17. Within the terminology adopted here, the simple designation Hartree-Fock (HF) in the literature most often refers to our restricted HF (RHF), in particular in atomic physics and the physics of the homogeneous electron gas. In nuclear physics, however, the simple designation HF most often refers to a space (S)-UHF. The simple designation unrestricted Hartree-Fock (UHF) in Chemistry most often refers to our s-UHF.
18. A 3D magnetic-field-free version of the TCO has been used in the description of ssion in metal clusters [C. Yannouleas and U. Landman, *J. Phys. Chem.* **99**, 14 577 (1995); C. Yannouleas et al., *Comments At. Mol. Phys.* **31**, 445 (1995)] and nuclei [J. Manuh and W. Greiner, *Z. Phys.* **251**, 431 (1972); C. Y. Wong, *Phys. Lett.* **30B**, 61 (1969)].
19. See (a) section 3.8.4 in A. Szabo and N. S. Ostlund, *Modern Quantum Chemistry* (McGraw-Hill, New York, 1989); (b) J. A. Pople and R. K. Nesbet, *J. Chem. Phys.* **22**, 571 (1954).
20. The parameter controlling the appearance of electron localization within each individual dot is  $R_W = Q/\hbar\omega_0$ , where  $Q$  is the Coulomb interaction strength and  $\hbar\omega_0$  is the characteristic energy of the parabolic confinement;  $Q = e^2/\epsilon_0$ , with  $\epsilon_0 = (\hbar m \omega_0)^{-1}$  being the spatial extent of the lowest state's wave function in the parabolic confinement. Within the s-UHF, we find that Wigner crystallization occurs in both the single QD's and QDM's for  $R_W > 1$ . For  $\epsilon_0 = 20$ , one has  $R_W = 0.95$ .
21. See section 3.8 in Ref. [9](a).
22. M. Koskinen, M. Manninen, and S. M. Reimann, *Phys. Rev. Lett.* **79**, 1389 (1997).
23. P. O. Lowdin, *Phys. Rev. B* **97**, 1509 (1955); *Rev. Mod. Phys.* **36**, 966 (1964).
24. R. Pauncz, *Alternant Molecular Orbital Method* (W. B. Saunders Co., Philadelphia, 1967).
25. H. Heitler and F. London, *Z. Phys.* **44**, 455 (1927).
26. C. A. Coulson, *Valence* (Oxford University Press, London, 1961).
27. J. N. Murrell, S. F. Kettle, and J. M. Tedder, *The Chemical Bond* (Wiley, New York, 1985).
28. The early electronic model of valence was primarily developed by G. N. Lewis who introduced a symbolism where an electron was represented by a dot, e.g.,  $H \cdot H$ , with a dot between the atomic symbols denoting a shared electron. Later in 1927 Heitler and London formulated the first quantum mechanical theory of the pair-electron bond for the case of the hydrogen molecule. The theory was subsequently developed by Pauling and others in the 1930's into the modern theory of the chemical bond called the Valence Bond Theory.
29. Refs. [15,16] have studied, as a function of the magnetic field, the behavior of the singlet-triplet splitting of the QD  $H_2$  by diagonalizing the two-electron Hamiltonian inside them in a four-dimensional basis formed by the products  $\phi_L(r_1)\phi_L(r_2)$ ,  $\phi_L(r_1)\phi_R(r_2)$ ,  $\phi_R(r_1)\phi_L(r_2)$ ,  $\phi_R(r_1)\phi_R(r_2)$  of the 1s orbitals of the separated QD's. This Hubbard-type method [15] (as well as the refinement employed by Ref. [16] of enlarging the minimal two-electron basis to include the p orbitals of the separated QD's) is an improvement over the simple HLL method (see Ref. [15]), but apparently it is only appropriate for the weak-coupling regime at sufficiently large distances and/or interdot barriers. Our method is free of such limitations, since we employ an interdot-distance adjustable basis (see section 2) of at least 66 spatial TCO molecular orbitals when solving for the s-UHF ones. Even with consideration of the symmetries, this amounts to calculating a large number of two-body Coulomb matrix elements, of the order of  $10^6$ .
30. More precisely our GVB method belongs to a class of Projection Techniques known as Variation before Projection, unlike the familiar in chemistry GVB method of Goddard and coworkers [W. A. Goddard III et al., *Acc. Chem. Res.* **6**, 368 (1973)], which is a Variation after Projection [see P. Ring and P. Schuck, *The Nuclear Many-Body Problem* (Springer, New York, 1980) ch. 11].
31. see section 3.8.7 in Ref. [9].
32. Symmetry breaking in coupled QD's within the LSD has been explored by J. Kolehmainen et al. [*Eur. Phys. J. D* **13**, 731 (2000)]. However, unlike the HF case for which a fully developed theory for the restoration of symmetries has long been established (see, e.g., the book by Ring and Schuck in Ref. [30]), the breaking of space symmetry within the spin-dependent density functional theory poses a serious dilemma [J. P. Perdew et al., *Phys. Rev. A* **51**, 4531 (1995)]. This dilemma has not been fully resolved to date; several remedies (like Projection, ensembles, etc.) are being proposed, but none of them appears to be completely devoid of inconsistencies [A. Savin in Recent developments and applications of modern density functional theory, edited by J. M. Seminario (Elsevier, Amsterdam, 1996) p. 327]. In addition, due to the unphysical self-interaction error, the density-functional theory is more resistant against symmetry breaking [see R. Bauernschmitt and R. Ahlrichs, *J. Chem. Phys.* **104**, 9047 (1996)] than the s-UHF, and thus it fails to describe a whole class of broken symmetries involving electron localization, e.g., the formation at  $B = 0$  of Wigner molecules in QD's (see footnote 7 in Ref. [7]), the hole trapping at Al impurities in silica [J. Laegsgaard and K. Stokbro, *Phys. Rev. Lett.* **86**, 2834 (2001)], or the interaction driven localization-delocalization transition in d- and f-electron systems, like Plutonium [S. Y. Savrasov et al., *Nature* **410**, 793 (2001)].

This figure "qdmdiss\_fig1.gif" is available in "gif" format from:

<http://arxiv.org/ps/cond-mat/0107014v1>



This figure "qdmdiss\_fig2.gif" is available in "gif" format from:

<http://arxiv.org/ps/cond-mat/0107014v1>

This figure "qdmdiss\_fig3.gif" is available in "gif" format from:

<http://arxiv.org/ps/cond-mat/0107014v1>

This figure "qdmdiss\_fig4.gif" is available in "gif" format from:

<http://arxiv.org/ps/cond-mat/0107014v1>